NASA CONTRACTOR REPORT

NASA CR-1028

NASA CR-1028

GPO PRICE $ _____

CFSTI PRICE(S) $ _____

Hard copy (HC) 3.00

Microfiche (MF) .65

ff 653 July 65

EXPERIM[illegible] INVESTIGATION OF RAD[illegible] IN JET-I[illegible] ROTATI[illegible] WATER

by Arthur [illegible]

Prepared by
UNITED AI[illegible]
East Hartford[illegible]
for
NATIONAL AE[illegible]

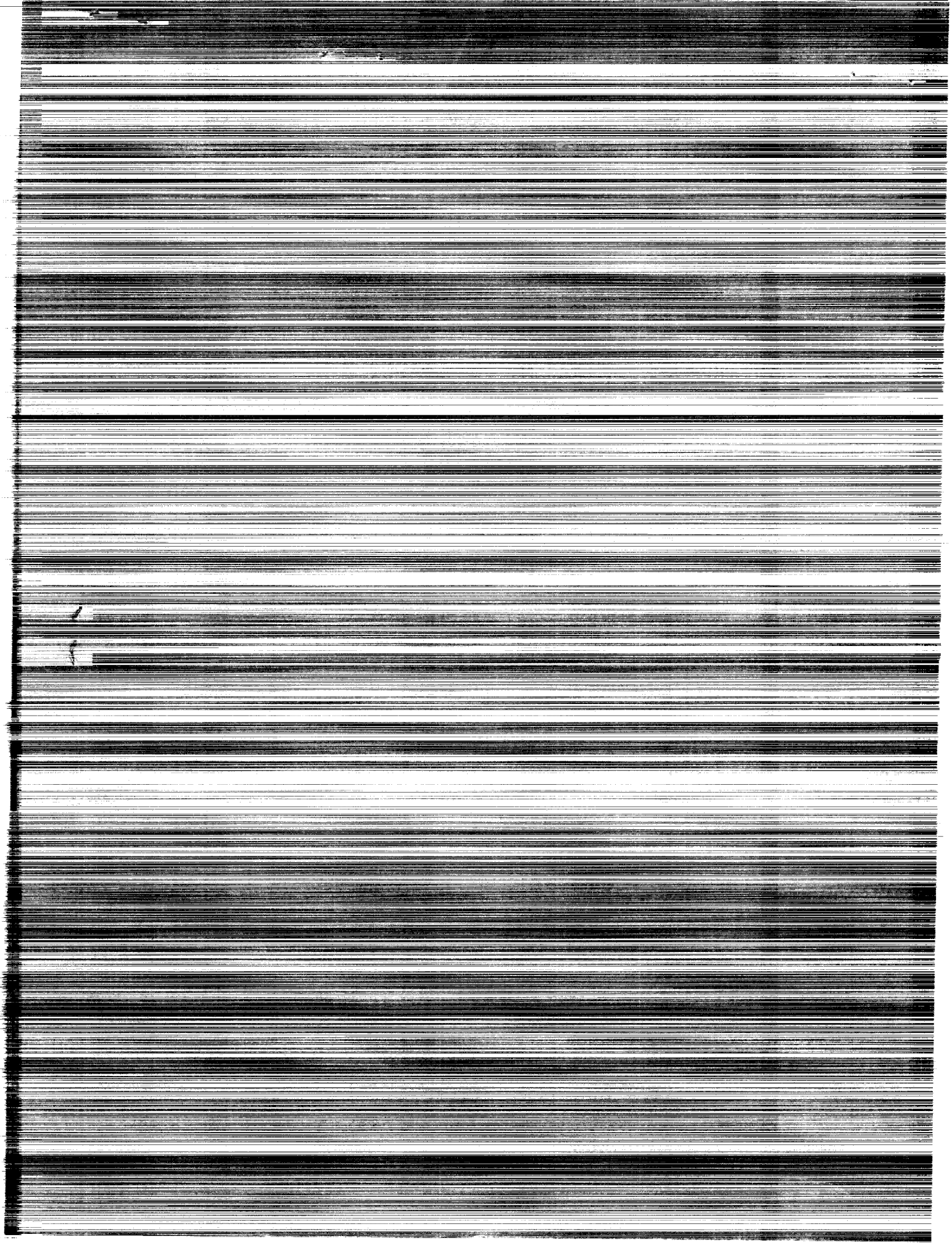

NASA CR-1028

EXPERIMENTAL INVESTIGATION OF RADIAL-INFLOW VORTEXES IN JET-INJECTION AND ROTATING-PERIPHERAL-WALL WATER VORTEX TUBES

By Arthur Travers

Issued by Originator as Report No. F-910091-14

Prepared under Contract No. NASw-847 by
UNITED AIRCRAFT CORPORATION
East Hartford, Conn.

for

NATIONAL AERONAUTICS AND SPACE ADMINISTRATION

For sale by the Clearinghouse for Federal Scientific and Technical Information
Springfield, Virginia 22151 – CFSTI price $3.00

Experimental Investigation of Radial-Inflow Vortexes in Jet-Injection and Rotating-Peripheral-Wall Water Vortex Tubes

TABLE OF CONTENTS

Experimental Investigation of Radial-Inflow Vortexes in Jet-Injection and Rotating-Peripheral-Wall Water Vortex Tubes

SUMMARY

Experiments were conducted in water vortex tubes to determine the effects of peripheral-wall injection area and axial bypass on the flow pattern and location of the radial stagnation surface in radial-inflow vortexes. The particular type of flow pattern investigated contains a central cell region which is bounded on the outside by a radial stagnation surface which appears to be laminar. At the radius of the radial stagnation surface, all radial flow passes through the end wall boundary layers. The flow in the vortex is laminar for radii less than that of the radial stagnation surface and is turbulent at larger radii.

Two 10-in.-dia by 30-in.-long lucite vortex tubes were used: a jet-injection vortex tube and a rotating-peripheral-wall vortex tube. In tests with the jet-injection vortex tube, flow was injected through the peripheral-wall and was removed (1) through two axial bypass exhaust annuli (a 1/8-in.-wide annulus was located at the outer edge of each end wall) and two 1.0-in.-dia thru-flow ports located at the centers of the end walls, or (2) through only the thru-flow ports. This vortex tube was tested with different peripheral-wall injection areas. In tests with the rotating-peripheral-wall vortex tube where there was no provision for axial bypass, the flow was injected through the rotating peripheral wall and was withdrawn through the thru-flow ports.

Tests were conducted with different combinations of tangential injection and radial Reynolds numbers, different amounts of bypass flow, and different peripheral-wall injection areas. The characteristics of the flow and the radius of the radial stagnation surface were determined from observations and photographs of dye patterns. The results of the experiments were compared with the results of a previous theoretical investigation of confined vortex flows.

RESULTS

1. In the jet-injection vortex tube with no bypass, vortex flow patterns with laminar radial stagnation surfaces were obtained using small peripheral-wall injection areas. The ratio of the radius of the radial stagnation surface to the radius of the vortex tube, r_s/r_o, increased as the peripheral-wall injection area was decreased.

2. In the jet-injection vortex tube with axial bypass, r_s/r_o increased with decreasing radial Reynolds number for constant peripheral-wall injection flow rate, i.e., r_s/r_o increased with increasing percent bypass flow. The maximum ratio of r_s/r_o at which laminar radial stagnation surfaces were observed was 0.7.

3. In the jet-injection vortex tube with axial bypass, axial waves were observed along the laminar radial stagnation surface for $\overline{V}_z/V_{\phi,P} > 0.02$, i.e., when the average axial velocity in the region outside of the radial stagnation surface was greater than about 2 percent of the tangential (circumferential) velocity at the peripheral wall.

4. In the rotating-peripheral-wall vortex tube without bypass, laminar radial stagnation surfaces were observed at values of r_s/r_o as large as 0.89. This increase relative to the values measured in the jet-injection vortex tube is attributable to the reduction in turbulence near the peripheral wall due to the decreased wall shear and the absence of injection jets.

5. The trends observed in the variation of r_s/r_o in both the jet-injection and rotating-peripheral-wall vortex tubes agree with those predicted by theory.

6. In the jet-injection vortex tube, the ratio of the tangential velocity at the peripheral wall (after the injected flow has been slowed down by diffusion, jet mixing and peripheral-wall friction) to the average tangential injection velocity decreased with decreasing peripheral-wall injection area.

INTRODUCTION

An experimental and theoretical investigation of gaseous nuclear rocket technology is being conducted by the United Aircraft Research Laboratories under Contract NASw-847 administered by the joint AEC-NASA Space Nuclear Propulsion Office. The research performed under this contract is primarily directed toward the vortex-stabilized nuclear light bulb engine concept.

In this concept (Fig. 1a), the propellant is heated by thermal radiation passing through an internally-cooled transparent wall located between the gaseous nuclear fuel and the propellant. A buffer gas is injected tangent to the inner surface of the transparent peripheral wall to drive a vortex. The primary reason for using a vortex flow is to prevent nuclear fuel and fission products from coming into contact with the transparent wall.

Previous fluid mechanics experiments have indicated that a radial-inflow vortex appears especially promising for this application. Many of the characteristics of radial-inflow vortexes have been investigated in previous studies at United Aircraft (Refs. 1 through 14) and elsewhere (Refs. 15 through 19). The particular radial-inflow pattern of interest for the nuclear light bulb engine is illustrated in Fig. 1b. It is characterized by a laminar radial stagnation surface across which there is no radial convection. A central recirculation-cell region occurs inside of the radial stagnation surface, and a region of axial flow toward the end walls occurs outside the radial stagnation surface. At the radius of the radial stagnation surface, all of the radial flow passes through the end-wall boundary layers. Previous flow visualization studies in jet-injection vortex tubes (Refs. 2, 5, 6, 7, and 10) have shown that the flow is essentially laminar at radii less than that of the radial stagnation surface and is turbulent at larger radii. The turbulence outside of the radial stagnation surface is due in part to wall shear and jet mixing. It is expected that the stabilizing effect of the radial temperature gradient in a nuclear light bulb engine would reduce the turbulence observed in the outer region in these constant-temperature laboratory experiments (see discussion in Ref. 14). The central laminar-flow region would be suitable for fuel containment in the engine, and the axial flow in the outer region would carry away fuel and fission products that diffuse radially outward.

According to the theoretical investigation reported in Ref. 1, radial stagnation surfaces and cells occur when the secondary flow resulting from friction on the end walls and the radial gradient of pressure in the vortex is greater than the flow withdrawn through the thru-flow ports at the centers of the end walls. A secondary-flow similarity parameter, $\beta_t = (D/L)(Re_{t,p}{}^{0.8}/Re_r)$, was introduced in Ref. 1. In this expression, D and L are the diameter and length of the vortex tube, $Re_{t,p}$ is the tangential Reynolds number (a measure of the tangential velocity at the periphery of the tube), and Re_r is the radial Reynolds number (a measure of the mass flow withdrawn through the thru-flow ports). The magnitude of the

parameter β_t provides an indication of the type of flow pattern that will occur. The three general types of flow patterns and the corresponding ranges of values of β_t are shown in Fig. 2. The flow regime of interest in this investigation is shown at the top of Fig. 2; it occurs for values of β_t greater than about 25. Ref. 1 also indicates that in this flow regime the radius of the radial stagnation surface increases with increasing β_t.

The jet-injection vortex tubes used in previous flow visualization studies (Refs. 2, 5, 6, 7, and 10) were designed with large peripheral-wall injection areas. This allowed large amounts of flow to be injected into the vortex tube to overcome the momentum losses due to peripheral-wall shear and jet mixing. However, if all of the injected flow were withdrawn through the thru-flow ports, the ratio $Re_{t,p}^{0.8}/Re_r$ would be small, and values of β_t considerably less than 25 would result. Therefore, to establish radial stagnation surfaces with these large injection areas, it was necessary to remove a large fraction of the injected flow before it moved radially inward into the vortex. This permitted the amount of flow withdrawn through the thru-flow ports to be reduced. Thus, Re_r was decreased, the ratio $Re_{t,p}^{0.8}/Re_r$ was increased, and values of β_t greater than 25 were obtained.

The removal of a large fraction of the injected flow was accomplished using the peripheral bypass configuration shown in Fig. 3a. However, it would be undesirable in a nuclear light bulb engine to remove bypass flow through the peripheral wall because of interference with the transparent wall configuration and the added complication of extensive ducting. Bypass flow could be removed through an annular exhaust (axial bypass) at one or both ends of the engine as indicated in Fig. 3b. In this case, it would be desirable to minimize the amount of bypass flow necessary for the establishment of a flow pattern with a laminar radial stagnation surface (to minimize the ducting and load on the fuel recycle system). Ideally, it would be best to operate without any bypass flow at all. This appeared to be possible if the ratio $Re_{t,p}^{0.8}/Re_r$ could be increased by using very small peripheral-wall injection areas which would result in larger values of $Re_{t,p}$ for a given Re_r.

Accordingly, the objectives of the investigation reported herein were (1) to determine the effects of peripheral-wall injection area and axial bypass on the stability of the flow and the location of the laminar radial stagnation surface in jet-injection vortex tubes, (2) to determine whether or not the desired vortex flow patterns can be obtained without bypass in jet-injection vortex tubes, and (3) to determine the influence of the peripheral-wall turbulent mixing region present in jet-injection vortex tubes on the location of the radial stagnation surface.

DESCRIPTION OF EQUIPMENT AND PROCEDURES

Description of Test Equipment

Vortex Tubes

Two transparent-wall water vortex tubes, one the jet-injection vortex tube of Ref. 10 and the other the rotating-peripheral-wall vortex tube of Ref. 20, were used in this investigation. Photographs of the apparatus are shown in Figs. 4 and 5, respectively.

Jet-Injection Vortex Tube

The jet-injection vortex tube (Fig. 4) consisted of a 10-in.-dia by 30-in.-long lucite tube with 2144 injection ports of 0.060-in.-dia. These ports were in 119 staggered circumferential rows (60 rows of 20 ports and 59 rows of 16 ports). The injection angle for all ports was 19 deg measured with respect to the tangent at the wall at the point of injection. Peripheral bypass plenums extending the full length of the vortex tube were located at 90-deg intervals around the peripheral wall. This 10-in.-dia tube was mounted concentrically in a 14-in.-dia lucite tube so that the annular volume between the two tubes served as an injection plenum. The peripheral bypass plenums used in the investigation in Ref. 10 were not used in the present investigation; however, some of the data obtained during the investigation of Ref. 10 are presented herein for comparison.

Experiments were conducted in the jet-injection vortex tube with axial bypass for four different peripheral-wall injection areas (A_j = 0.118, 0.236, 0.679 and 6.0 in.^{2}). The peripheral-wall injection area was decreased from 6.0 in.^{2} by blocking the required number of injection ports with modeling clay. Details of the vortex tube, bypass geometry and peripheral-wall injection geometries are shown in Fig. 6a. Lucite end walls, each having a 1/8-in.-wide annulus for axial bypass at its outer edge and a 1.0-in.-dia thru-flow port at the center, were used. Flow was injected into the vortex tube through the peripheral-wall injection ports and was withdrawn either (1) through the axial bypass and thru-flow ports, or (2) through only the thru-flow ports.

Rotating-Peripheral-Wall Vortex Tube

The rotating-peripheral-wall vortex apparatus (Fig. 5) contained a 10-in.-ID by 30-in.-long rotating lucite cylinder (the peripheral wall of the vortex tube) having 16,000 holes of 0.062-in.-dia drilled normally through the wall. This rotating peripheral wall was surrounded by a 14-in.-ID stationary lucite cylinder that formed a plenum for injecting water through the holes in the peripheral wall. The peripheral wall was driven by a 3/4-hp d-c motor with a variable-speed controller which regulated rotational speed to ±1 percent from 40 to 456 rpm. The

end-wall drive spool (see Fig. 5) could be locked to the peripheral-wall drive or to the test stand. This allowed the end walls to be rotated with the peripheral wall or held stationary.

Due to the independent control of $Re_{t,o}$ and Re_r, radial stagnation surfaces can be established without bypass in this vortex tube. Moreover, the turbulence level near the peripheral wall is low due to the absence of large amounts of wall shear and jet mixing.

Experiments were conducted in the rotating-peripheral-wall vortex tube without bypass and with stationary end walls. Additional details of the vortex tube are shown in Fig. 6b. Plain lucite end walls with 1.0-in.-dia thru-flow ports at their centers were used. Flow was injected into the vortex tube through the injection ports in the rotating peripheral wall and withdrawn through the thru-flow ports at the centers of the end walls.

Flow Control System

Water was pumped from a storage tank through the injection plenums into the vortex tubes. The desired flow conditions were obtained by adjustment of control valves downstream of the thru-flow ports and downstream of the axial bypass plenums. Measurements of the total flow injected into the vortex tube were made using a turbine flowmeter located in the inlet flow pipe leading to the injection plenums. The thru-flow rate was determined in a similar manner by measuring the flow rate leaving the end-wall thru-flow ports. Measurements of water temperature were made using a thermometer located in the storage tank to determine the actual kinematic viscosity for calculating Reynolds numbers.

Optical System and Flow Visualization Techniques

Flow visualization was provided by injection of fluorescent dye into the vortex through ports in the end walls or ports in the peripheral wall at the axial mid-plane. A sketch of the optical system used to photograph dye patterns is shown in Fig. 7. Photographs of dye patterns were taken through an end wall with illumination through an adjustable slit (usually 1/4-in.-wide) located at the axial mid-plane of the vortex tube. Time exposure photographs of the dye patterns were also taken through the side wall of the vortex tube by interchanging the locations of the camera and light source. A microflash lamp having a 0.1-microsecond flash period was used as the light source for photographs of dye patterns taken through the end wall. The mercury vapor lamp used as the light source for the photographs taken through the side wall was powered by a 1-kw d-c power supply.

Tangential velocities in the primary-flow region of the jet-injection vortex tube were measured for some flow conditions. The velocities were determined from time-exposure photographs of neutrally buoyant polystyrene spheres injected into the flow through a special port located in the peripheral wall at the axial

mid-plane of the vortex tube. The optical system shown in Fig. 7 was also used to photograph the particles. The chopping disc contained 20 or 40 slots, depending on the flashing rate desired, and was driven by a variable-speed d-c shunt motor which allowed the flashing rate to be varied from 60 to 3000 flashes per second. Intermittent illumination of the suspended particles caused them to appear as a series of streaks on a time exposure (see typical particle-trace photograph in Fig. 8). This technique permitted quantitative evaluation of the tangential velocities within the vortex without using probes which would disturb the flow.

Description of Test and Data Reduction Procedures

Test Procedures and Range of Flow Conditions Investigated

A typical series of flow visualization tests using the jet-injection vortex tube was conducted in the following manner. With a fixed peripheral-wall injection area (A_j) and jet-injection flow rate (Q_j), the bypass flow rate was changed so that the percent bypass ($(Q_{BP}/Q_j) \times 100$) varied between 0 and 100%. As the percent bypass increased the amount of flow withdrawn through the thru-flow ports (Q_t) was decreased ($Q_j = Q_{BP} + Q_t$).

The pertinent flow parameters specified in these tests were the tangential injection and radial Reynolds numbers. The tangential injection Reynolds number is defined as

$$Re_{t,j} = \frac{V_j r_o}{\nu} \tag{1}$$

where V_j is the average tangential injection velocity, r_o is the radius of the vortex tube, and ν is the kinematic viscosity for the water temperature at the time the tests were conducted. In this test program, $Re_{t,j}$ was varied from 80,000 to 1,800,000.

The radial Reynolds number is defined as

$$Re_r = \frac{Q_t}{2\pi\nu L} \tag{2}$$

where Q_t is the total volumetric flow rate of fluid withdrawn through the thru-flow ports at the centers of the end walls and L is the vortex tube length. Values of Re_r from 20 to 442 were investigated.

As will be shown, the ratio of the average local velocity near the peripheral wall to the jet-injection velocity varied markedly with peripheral-wall injection area. Consequently, a more meaningful tangential Reynolds number based on average flow conditions at the peripheral wall rather than at the jets was also calculated

for the tests in the jet-injection vortex tube. This tangential Reynolds number is defined as

$$Re_{t,p} = \frac{V_{\phi,P} r_o}{\nu} \tag{3}$$

where $V_{\phi,P}$ is the tangential velocity at the peripheral-wall determined by extrapolating the measured tangential velocity profiles (obtained by the particle-trace method) to the peripheral wall. A sketch illustrating this extrapolation is shown in the insert of Fig. 9. Data indicating the approximate variation of $V_{\phi,P}/V_j$ with peripheral-wall injection area are shown in Fig. 9. Although insufficient data were obtained to define the curve shown in Fig. 9, the curve must have the shape shown (asymptotic to $V_{\phi,P}/V_j = 1.0$ at large values of A_j). In this program, $Re_{t,p}$ ranged from 47,500 to 262,000.

Typical tests in the rotating-peripheral-wall vortex tube were conducted by varying the peripheral-wall rotational speed (N_o) between 40 and 145 rpm with a fixed volumetric flow rate (Q_j) through the peripheral wall. The flow parameters specified in these tests were also the tangential and radial Reynolds numbers. The tangential Reynolds number in the rotating peripheral-wall vortex tube is defined as

$$Re_{t,o} = \frac{\pi N_o r_o^2}{30\nu} \tag{4}$$

In this program, $Re_{t,o}$ was varied from 67,000 to 244,000. The radial Reynolds number is defined by Eq. (2); Re_r was varied from 97 to 154. Since there was no bypass, Q_t was equal to Q_j in all tests.

Comparisons of the results of the tests using the two different vortex tube configurations were made using calculated values of the secondary-flow parameter, β_t. As discussed previously, vortex flows having equal values of β_t have similar flow patterns (see Fig. 2 and Ref. 1). For the jet-injection and rotating-peripheral-wall vortex tubes, respectively, β_t is defined as

$$\beta_t = \frac{D}{L} \frac{(Re_{t,p})^{0.8}}{Re_r} = \frac{D}{L} \frac{(Re_{t,o})^{0.8}}{Re_r} \tag{5}$$

Although β_t was derived in Ref. 1 for flows without bypass, it is shown in the results presented in this report that this parameter provides an indication of the trends observed in the experiments even with axial or peripheral bypass. For the flow conditions investigated, β_t ranged from approximately 18 to approximately 128.

Reduction of Particle-Trace Data

The first step in the procedure for obtaining local tangential velocities in the primary-flow region was to determine the radius of a particle trace from a photograph (see Fig. 8). Two points at the ends of dashes were selected and the circumferential distance between them was calculated from the radius and the central angle subtended. The time of travel was determined from the number of dashes between the points and the light flashing rate. The tangential velocity was then calculated by dividing the circumferential distance by the time of travel. The photographs from which the tangential velocities were determined were all taken with light illumination at the axial mid-plane.

DISCUSSION OF RESULTS

Results of Tests in Jet-Injection Vortex Tube

Effects of Peripheral-Wall Injection Area and Axial Bypass on Location of Radial Stagnation Surface

Typical dye pattern photographs illustrating flow patterns in the jet-injection vortex tube are shown in Fig. 10. These and all other photographs in this report that were taken through an end wall show flow patterns at the axial mid-plane. In all photographs the flow rotation is counterclockwise, and the dye was injected either through ports in the end walls or through ports in the peripheral wall at the axial mid-plane.

The dye patterns shown in Fig. 10 illustrate the effect of axial bypass on the radius of the laminar radial stagnation surface. These results were obtained with one peripheral-wall injection area (A_j = 0.679 in.^{2}) and a constant tangential Reynolds number ($Re_{t,p}$ = 47,500). The radial stagnation surface appears as the distinct dye annulus at the end of the radial arrow, r_s. As the percent bypass ((Q_{BP}/Q_j) x 100) was increased from 0 to 65 percent, the ratio of the radius of the radial stagnation surface to the radius of the vortex tube, r_s/r_o, increased from 0.30 to 0.70. Since the percent bypass was increased while holding the tangential Reynolds number constant, the radial Reynolds number decreased from Re_r = 102.5 to 35.9 and the secondary flow parameter increased from β_t = 18.0 to 51.3. The trend of increasing r_s/r_o with increasing β_t shown in this example (Fig. 10) is in agreement with the theory of Ref. 1.

Figure 11 presents a summary of the effect of percent bypass on the radius of the laminar radial stagnation surface. The data for peripheral bypass are from Ref. 10. The data in Fig. 11 indicate three general trends: (1) for constant peripheral-wall injection area, r_s/r_o increased with increasing percent bypass; (2) for constant percent bypass, r_s/r_o increased with decreasing peripheral-wall injection area; and (3) for constant r_s/r_o, the percent bypass required decreased with decreasing peripheral-wall injection area. This latter trend is of particular interest for the nuclear light bulb engine where it is desired to establish a radial stagnation surface at a large radius with little or no bypass.

The trend of decreasing percent bypass required to obtain the same r_s/r_o as peripheral-wall injection area decreases would be expected based on consideration of the secondary flow parameter, β_t. Peripheral-wall injection area does not enter into the development of the theory of Ref. 1. According to the theory, two vortex flows having the same β_t will have approximately the same r_s/r_o, regardless of peripheral-wall injection area. (For a given β_t, there is a very small effect of changes in Re_r on r_s/r_o, but this effect is negligible.) The equation for β_t

(Eq. (5)) may be written as

$$\beta_t = \frac{D}{L} \cdot \frac{(Re_{t,p})^{0.8}}{Re_r} = \frac{2\pi\nu D}{Q_j} \cdot \left(\frac{Q_j r_o}{\nu}\right)^{0.8} \cdot \frac{\left(\frac{Re_{t,p}}{Re_{t,j}} \cdot \frac{1}{A_j}\right)^{0.8}}{1 - Q_{BP}/Q_j} \qquad (6)$$

As shown in Fig. 9, the ratio $Re_{t,p}/Re_{t,j}$ decreases with decreasing A_j. The following values of the parameter $(Re_{t,p}/Re_{t,j})/A_j$, which appears in the numerator of Eq. (6), were calculated using the data points in Fig. 9:

A_j, in.^{2}	$(Re_{t,p}/Re_{t,j})/A_j$, in.$^{-2}$
6.00	0.15
0.679	0.49
0.236	0.89
0.118	1.02

This table indicates that when the injection flow rate (Q_j) remains constant, the numerator of Eq. (6) increases as A_j decreases. To maintain β_t constant so that r_s/r_o remains constant, the denominator must also increase as A_j decreases. This in turn implies that the percent bypass ($(Q_{BP}/Q_j) \times 100$) must decrease, which is the result obtained in the experiments (Fig. 11).

The maximum value of r_s/r_o that could be obtained with axial bypass was about 0.7 for all four injection areas tested (see Fig. 11). The maximum radial extent of the laminar radial stagnation surface appeared to be limited by the width of the turbulent mixing region near the peripheral wall. With small increases in percent bypass over the values at the right ends of the curves in Fig. 11, no increase in r_s/r_o was observed. Instead, the radial stagnation surface began to deform elliptically as shown in Fig. 10d. With further increases in percent bypass, the laminar radial stagnation surface deteriorated, and no radial stagnation surface was discernable.

Under certain flow conditions with axial bypass, disturbances in the form of traveling waves in the laminar radial stagnation surface were observed. These waves ran in the lengthwise direction in the vortex tube and appeared to be caused by high axial shear. Associated with the waves were regions of increased turbulence near the end walls. Typical dye patterns illustrating the effect of these waves on the radial stagnation surface are shown in Fig. 12. The radial stagnation surface became rippled and increased turbulence was noted in the region outside the stagnation surface near both end walls. A summary of the flow conditions for which

the waves were observed is presented in Fig. 13. In Fig. 13, the ratio of the average axial velocity outside the radial stagnation surface close to the ends of the vortex tube to the tangential (circumferential) velocity at the peripheral wall, $\overline{V}_Z/V_{\phi,P}$, is the ordinate and percent bypass is the abscissa. Data are shown for all peripheral-wall injection areas and bypass configurations that were tested. Data from tests in the rotating-peripheral-wall vortex tube are also shown (these tests are discussed in a later section). Axial waves in the laminar radial stagnation surface were observed for values of $\overline{V}_Z/V_{\phi,P} > 0.02$ (above the shaded boundary in Fig. 13), i.e., when the average axial velocity was greater than about 2 percent of the tangential velocity at the peripheral wall. As indicated in the figure, these waves were observed only with axial bypass in the jet-injection vortex tube with $A_j = 0.679$ and 6.0 in.^{2}. Note the large differences in the values of $\overline{V}_Z/V_{\phi,P}$ for $A_j = 6.0$ in.^{2} with peripheral and axial bypass (compare solid circles with open circles). Also note the differences in the measured values of r_s/r_o for these two configurations in Fig. 11. Consequently, for the largest peripheral-wall injection area tested, axial bypass had generally less desirable fluid mechanics characteristics than peripheral bypass because it resulted in lower values of r_s/r_o and, under some conditions, caused waves in the radial stagnation surface.

Effect of Peripheral-Wall Injection Area on Location of Radial Stagnation Surface without Bypass

Figure 11 indicates that laminar radial stagnation surfaces can be obtained without bypass if the peripheral-wall injection area is made small enough. The data show that with zero-percent bypass the maximum extent of the radial stagnation surface was $r_s/r_o = 0.64$ for the range of conditions tested. This was obtained using the smallest injection area available at the time of the tests, $A_j = 0.118$ in.^{2}.

In previous tests using jet-injection vortex tubes (Refs. 5, 6, 7, and 10) where a large injection area was used ($A_j = 6.0$ in.^{2}), flows with laminar radial stagnation surfaces could not be obtained without bypass. These flows had values of β_t less than 10 and were turbulent from the centerline of the vortex tube to the peripheral wall. In the present test program, laminar radial stagnation surfaces were obtained without bypass for injection areas of $A_j = 0.679$ in.^{2} and less. Typical dye patterns showing the effect of decreasing injection area for constant radial Reynolds number are presented in Fig. 14. The ratio r_s/r_o increased from 0.3 to 0.64 as the peripheral-wall injection area was decreased from $A_j = 0.679$ in.^{2} to 0.118 in.^{2}. It is interesting to note that the calculated value of β_t for Fig. 14a is only 18 while theory predicts that a radial stagnation surface would not occur for β_t less than about 26 for $Re_r = 102.5$ (see Fig. 2). This illustrates that although changes in β_t provide a reasonably good indication of the trends observed in the experiments, there are uncertainties in the application of the theory and in the method used to calculate β_t (e.g., Fig. 9) which cause differences between the predicted and observed flow patterns.

Results of Tests in Rotating-Peripheral-Wall Vortex Tube

Tests were conducted in the rotating-peripheral-wall vortex tube without bypass to determine the effect of a reduction in turbulence near the peripheral wall on the radius of the laminar radial stagnation surface. The turbulence level is less in the rotating-peripheral-wall vortex tube than in the jet-injection vortex tube due to the absence of large amounts of wall shear and jet mixing. Thus, the hypothesis that the maximum radius of the radial stagnation surface is limited by turbulence near the peripheral wall can be investigated by comparing the results obtained in the two vortex tubes.

Dye patterns illustrating the effect of changes in the peripheral-wall rotation rate on the radius of the laminar radial stagnation surface for a constant radial Reynolds number (Re_r = 131) are shown in Fig. 15. As N_o was increased from 50 to 130 rpm, r_s/r_o increased from 0.62 to 0.85. This is the trend that would be expected since β_t increased from 21.9 to 46.7.

The results of all tests in the rotating-peripheral-wall vortex tube are summarized in Fig. 16. The maximum value measured was $r_s/r_o = 0.89$; larger values probably would have been measured if higher peripheral-wall rotation rates were used. The data indicate that r_s/r_o is strongly dependent upon β_t and weakly dependent upon Re_r, which are results expected on the basis of the theory of Ref. 1.

Values of the ratio $\overline{V}_Z/V_{\phi,o}$ for some of the flow conditions shown in Fig. 16 are given in Fig. 13. As would be expected since there was no axial bypass flow, $\overline{V}_Z/V_{\phi,P}$ was less than 0.02, and there was no evidence of axial waves in the radial stagnation surface.

Summary of Results and Comparison with Theory

A summary of the measured radii of the laminar radial stagnation surfaces in both vortex tubes and the theoretical results from Ref. 1 is shown in Fig. 17. This summary clearly illustrates that the main trend observed in all of the experiments agrees with the trend predicted by the theory; that is, r_s/r_o increases as β_t increases. It also indicates where the results are in apparent disagreement with the theory, and shows differences in the results obtained using the two different vortex tube configurations. For the case with a rotating peripheral wall, which closely approaches the assumptions of the theory, there is reasonable agreement; the main areas of disagreement are for some of the jet-injection vortex tube results.

One important result is that laminar radial stagnation surfaces were obtained at values of β_t less than about 25, i.e., below the minimum value of β_t for which radial stagnation surfaces would be expected on the basis of the theory. As mentioned previously, there are uncertainties in the application of the theory to

vortex tubes having axial or peripheral bypass because the theory was originally developed for vortex tubes without bypass. In addition, the accuracy of the empirical correlation of $Re_{t,p}/Re_{t,j}$ with A_j (Fig. 9) is also uncertain. The theory assumes that tangential shear in the primary-flow region is governed by laminar viscosity; this assumption is obviously not rigorous for the region outside the radial stagnation surface. The theory also employs as input quantities a series of formulas for tangential and radial shear on the end walls and for the shape of the tangential and radial velocity profiles in the end-wall boundary layers. These formulas cannot be any more accurate than other formulas employed in the analysis of turbulent boundary layers. Considering the limitations of the theory, the agreement between experiment and theory is surprisingly good.

Another important result is that the maximum value of r_s/r_o that could be obtained with axial bypass was 0.7. As β_t was increased beyond the values at the right ends of the curves in Fig. 17, the laminar radial stagnation surface deteriorated and was no longer discernable. In the jet-injection vortex tube with peripheral bypass, larger values of r_s/r_o were obtained (compare the curves with $A_j = 6.0$ in.^{2} in Fig. 17), although these values were not as large as would be expected on the basis of the calculated values of β_t. Moreover, larger values of r_s/r_o were obtained using the rotating-peripheral-wall vortex tube where the turbulence near the peripheral wall was considerably lower. This seems to support the hypothesis that turbulence near the peripheral wall limits the maximum radius of the laminar radial stagnation surface in jet-injection vortex tubes.

The conditions existing in the rotating-peripheral-wall vortex tube near the peripheral wall may be more representative of the conditions that would exist in a nuclear light bulb engine. It is expected that the density gradient caused by the radial gradient of temperature in the engine would reduce turbulence near the peripheral wall. This should allow a larger radius of the laminar radial stagnation surface to be obtained than could be obtained in the tests conducted during this program using the jet-injection vortex tube.

REFERENCES

1. Anderson, O.: Theoretical Solutions for the Secondary Flow on the End Wall of a Vortex Tube. United Aircraft Research Laboratories Report R-2494-1, prepared under Contract AF 04(611)-7448, November 1961.

2. Owen, F. S., R. W. Hale, B. V. Johnson, and A. Travers: Experimental Investigation of Characteristics of Confined Jet-Driven Vortex Flows. United Aircraft Research Laboratories Report R-2494-2, prepared under Contract AF 04(611)-7448, November 1961.

3. Anderson, O. L.: Theoretical Effect of Mach Number and Temperature Gradient on Primary and Secondary Flow in a Jet-Driven Vortex. Air Force Systems Command Report RTD-TDR-63-1098, prepared by United Aircraft Research Laboratories, November 1963.

4. Mensing, A. E., and J. S. Kendall: Experimental Investigation of Containment of Gaseous Iodine in a Jet-Driven Vortex. Air Force Systems Command Report RTD-TDR-63-1093, prepared by United Aircraft Research Laboratories, November 1963.

5. Johnson, B. V., A. Travers, and R. W. Hale: Measurements of Flow Patterns in a Jet-Driven Vortex. Air Force Systems Command Report RTD-TDR-63-1094, prepared by United Aircraft Research Laboratories, November 1963.

6. Travers, A., and B. V. Johnson: Measurements of Flow Characteristics in a Basic Vortex Tube. United Aircraft Research Laboratories Report C-910091-2, prepared under Contract NASw-847, September 1964. Also issued as NASA CR-278.

7. Travers, A., and B. V. Johnson: Measurements of Flow Characteristics in an Axial-Flow Vortex Tube. United Aircraft Research Laboratories Report C-910091-3, prepared under Contract NASw-847, September 1964. Also issued as NASA CR-277.

8. Johnson, B. V.: Analysis of Secondary-Flow-Control Methods for Confined Vortex Flows. United Aircraft Research Laboratories Report C-910091-1, prepared under Contract NASw-847, September 1964. Also issued as NASA CR-276.

9. Mensing, A. E., and J. S. Kendall: Experimental Investigation of Containment of a Heavy Gas in a Jet-Driven Light-Gas Vortex. United Aircraft Research Laboratories Report D-910091-4, prepared under Contract NASw-847, March 1965. Also issued as NASA CR-68931.

10. Travers, A.: Experimental Investigation of Peripheral-Wall Injection Techniques in a Water Vortex Tube. United Aircraft Research Laboratories Report D-910091-7, prepared under Contract NASw-847, September 1965. Also issued as NASA CR-68866.

11. McFarlin, D. J.: Experimental Investigation of the Effect of Peripheral-Wall Injection Technique on Turbulence in an Air Vortex Tube. United Aircraft Research Laboratories Report D-910091-5, prepared under Contract NASw-847, September 1965. Also issued as NASA CR-68867.

12. Johnson, B. V., and A. Travers: Analytical and Experimental Investigation of Flow Control in a Vortex Tube by End-Wall Suction and Injection. United Aircraft Research Laboratories Report D-910091-8, prepared under Contract NASw-847, September 1965. Also issued as NASA CR-68927.

13. Mensing, A. E., and J. S. Kendall: Experimental Investigation of the Effect of Heavy-to-Light-Gas Density Ratio on Two-Component Vortex Tube Containment Characteristics. United Aircraft Research Laboratories Report D-910091-9, prepared under Contract NASw-847, September 1965. Also issued as NASA CR-68926.

14. Clark, J. W., B. V. Johnson, J. S. Kendall, A. E. Mensing, and A. Travers: Summary of Gaseous Nuclear Rocket Fluid Mechanics Research Conducted Under Contract NASw-847. United Aircraft Research Laboratories Report F-910091-13, May 1967. Also AIAA Preprint No. 67-500, presented at AIAA Third Propulsion Joint Specialist Conference, Washington, D. C., July 17-21, 1967.

15. Rosenzweig, M. L., W. S. Lewellen, and D. H. Ross: Confined Vortex Flows with Boundary Layer Interaction. Aerospace Corporation Report No. ATN-64(9227)-2, February 20, 1964. Also AIAA Journal, Vol. 3, No. 12, December 1964, pp. 2127-2134.

16. Pivrotto, T. J.: Mass-Retention Measurements in a Binary Compressible Vortex Flow. Jet Propulsion Laboratory Technical Report No. 32-864, June 15, 1966.

17. Lewellen, W. S., M. L. Rosenzweig, and D. H. Ross: Effects of Secondary Flows on the Containment of a Heavy Gas in a Vortex. Aerospace Corporation Report No. TDR-469(9210-01)-3, 1965. Also AIAA Preprint No. 65-582, presented at AIAA Propulsion Joint Specialist Conference, Colorado Springs, Colorado June 14-18, 1965.

18. Chang, C. C., S. W. Chi, and C. M. Chen: Gas-Core Nuclear Rocket Fluid Mechanics Experiments at Catholic University of America. AIAA Preprint No. 67-502, presented at AIAA Third Propulsion Joint Specialist Conference, Washington, D. C., July 17-21, 1967.

19. Roschke, E. J.: Flow Visualization Studies of a Confined, Jet-Driven Water Vortex. Jet Propulsion Laboratory Technical Report No. 32-1004, September 16, 1966.

20. Travers, A.: Experimental Investigation of Flow Patterns in Radial-Outflow Vortexes Using a Rotating-Peripheral-Wall Water Vortex Tube. United Aircraft Research Laboratories Report F-910091-10, prepared under Contract NASw-847, May 1967. To be issued as NASA CR report.

LIST OF SYMBOLS

A_j	Total area of injection ports at peripheral wall of jet-injection vortex tube, ft^2 or $in.^2$
D	Diameter of vortex tube, ft or in.
L	Length of vortex tube, ft or in.
N_o	Peripheral-wall rotation rate, rpm
Q_{BP}	Total volumetric flow rate through axial bypass exhaust annuli or peripheral bypass ports, ft^3/sec
Q_j	Total volumetric flow rate injected through peripheral wall, ft^3/sec
Q_s	Secondary flow in one end-wall boundary layer, ft^3/sec
Q_t	Total volumetric flow rate through thru-flow ports, ft^3/sec or gpm
Q_z	Volumetric rate of flow toward one end wall through annular region between radial stagnation surface and peripheral wall; $Q_t/2$ for no-bypass and peripheral-bypass configurations, and $(Q_t + Q_{BP})/2$ for axial-bypass configurations; ft^3/sec
r	Local radius from centerline of vortex tube, ft or in.
r_o	Outer radius of vortex tube, ft or in.
r_s	Radius of radial stagnation surface, ft or in.
Re_r	Radial Reynolds number, $Q_t/2\pi\nu L$, dimensionless
$Re_{t,j}$	Tangential injection Reynolds number based on average injection velocity in jet-injection vortex tube, $V_j r_o/\nu$, dimensionless
$Re_{t,o}$	Tangential Reynolds number based on peripheral-wall rotational speed, $\pi N_o r_o^2/30\nu$, dimensionless
$Re_{t,p}$	Tangential Reynolds number based on velocity at peripheral wall of jet-injection vortex tube, $V_{\phi,p} r_o/\nu$, dimensionless
t	Time, sec

V_j Average tangential injection velocity in jet-injection vortex tube, Q_j/A_j, ft/sec

V_ϕ Tangential (circumferential) velocity of flow in vortex tube, ft/sec

$V_{\phi,O}$ Tangential velocity of rotating peripheral wall, $\pi N_o r_o/30$, ft/sec

$V_{\phi,P}$ Tangential velocity at peripheral wall of jet-injection vortex tube after injected flow has been slowed down by diffusion, jet mixing and peripheral-wall friction, ft/sec

$\overline{V}_Z$ Average axial velocity through annular region between radial stagnation surface and peripheral wall close to the ends of the vortex tube, $Q_z/\pi\,(r_o^2 - r_s^2)$, ft/sec

z Distance measured in a direction parallel to the axis of the vortex tube from the axial mid-plane, ft or in.

β_t Dimensionless secondary flow similarity parameter, $(D/L)\ Re_{t,p}{}^{0.8}/Re_r$ or $(D/L)\ Re_{t,o}{}^{0.8}/Re_r$

μ Laminar viscosity, lb-sec/ft^2

ν Laminar kinematic viscosity, ft^2/sec

ρ Density of water, slug/ft^3

ϕ Azimuthal coordinate

FIG. 1

SCHEMATIC DIAGRAMS OF NUCLEAR LIGHT BULB ENGINE AND DESIRED FLOW PATTERN

a) UNIT CAVITY OF NUCLEAR LIGHT BULB ENGINE

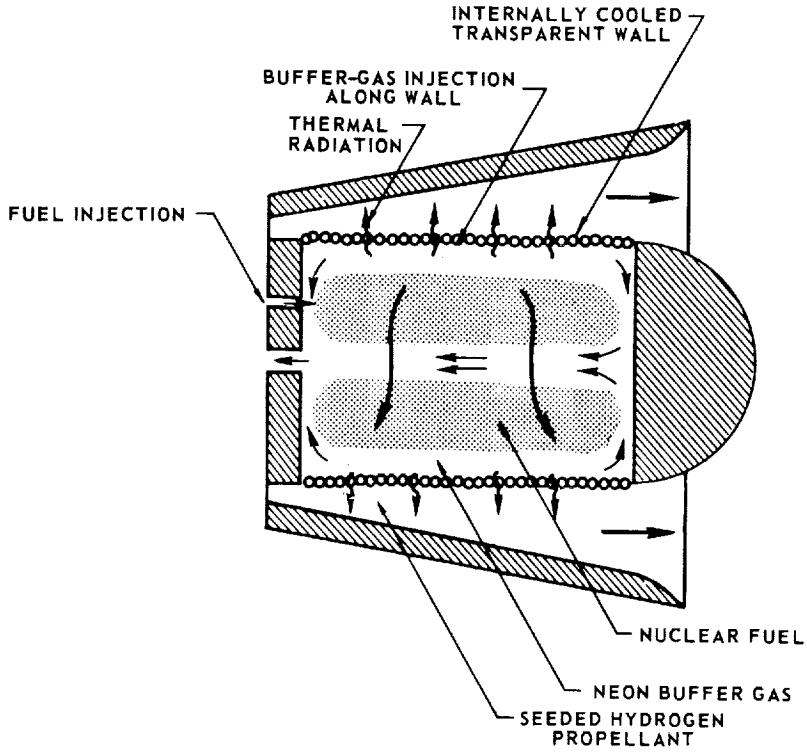

b) RADIAL-INFLOW FLOW PATTERN

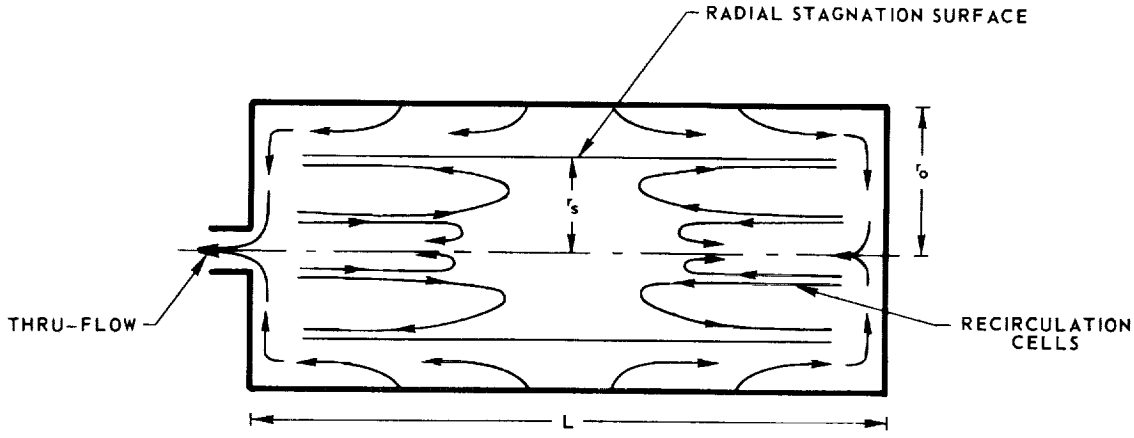

FIG. 2

SECONDARY FLOW REGIMES IN INCOMPRESSIBLE VORTEXES

FROM ANALYSIS OF REF. 1

SECONDARY FLOW PARAMETER, $\beta_t = \frac{D}{L} \frac{Re_{t,p}^{4/5}}{Re_r}$

(RADIUS OF VORTEX TUBE) / (RADIUS OF THRU-FLOW PORT) = 10

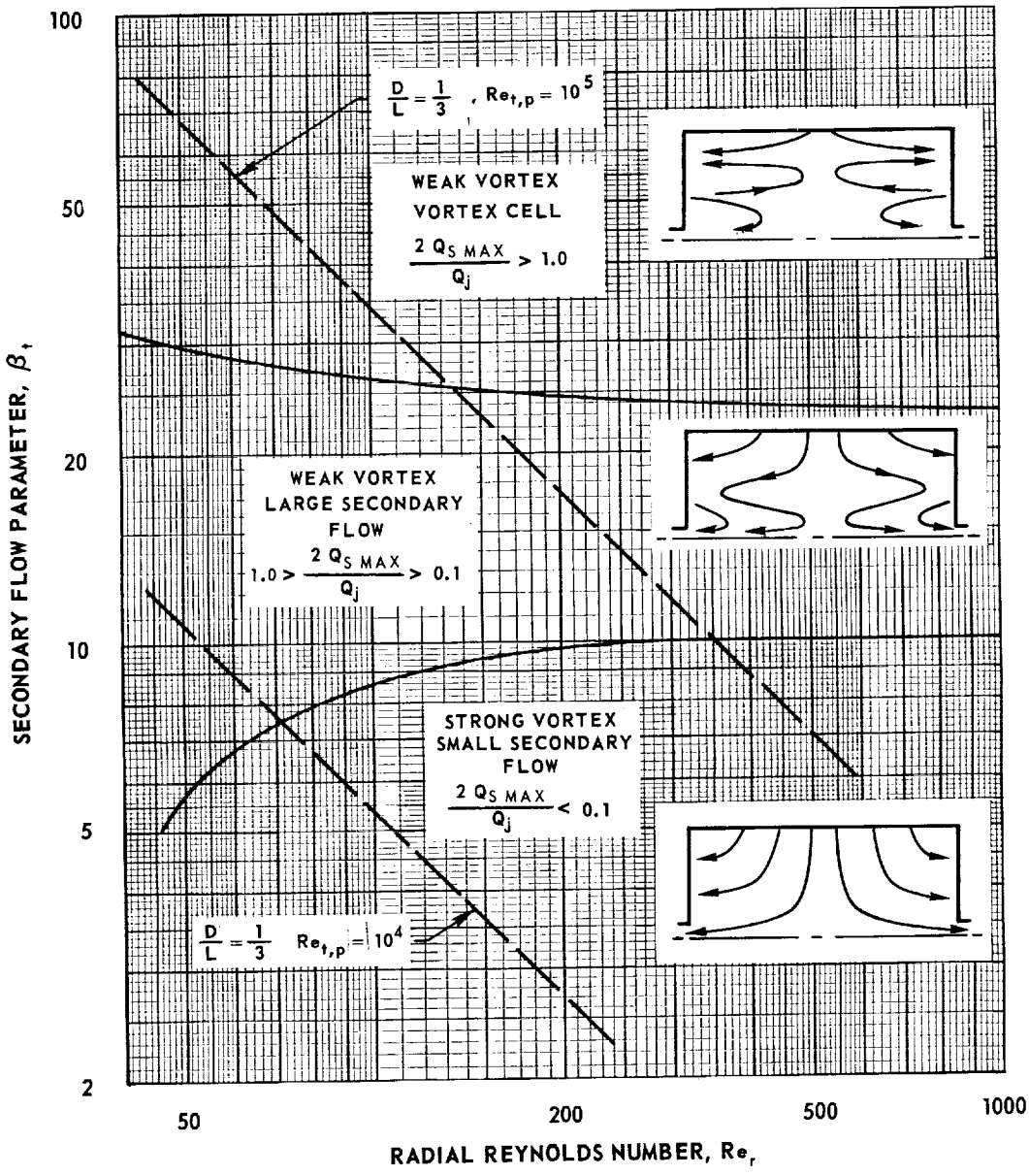

FIG. 3

SKETCHES OF PERIPHERAL BYPASS AND AXIAL BYPASS CONFIGURATIONS

NOTE: GEOMETRY IDENTICAL AT BOTH ENDS OF VORTEX TUBES

a) PERIPHERAL BYPASS CONFIGURATION

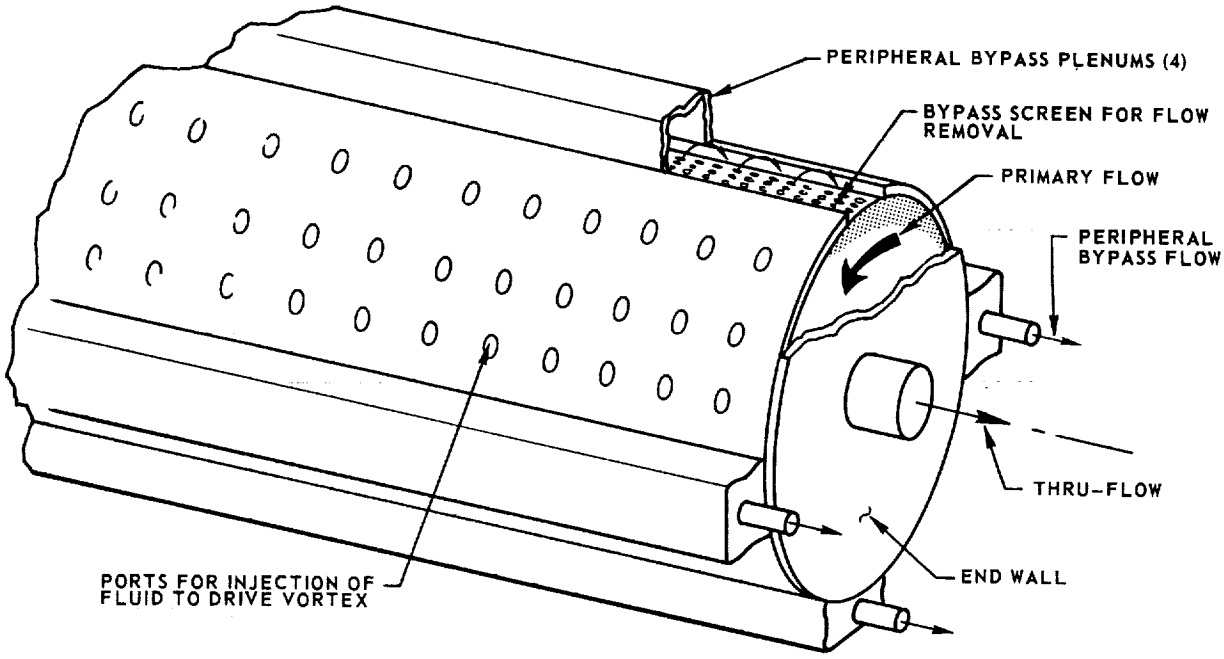

b) AXIAL BYPASS CONFIGURATION

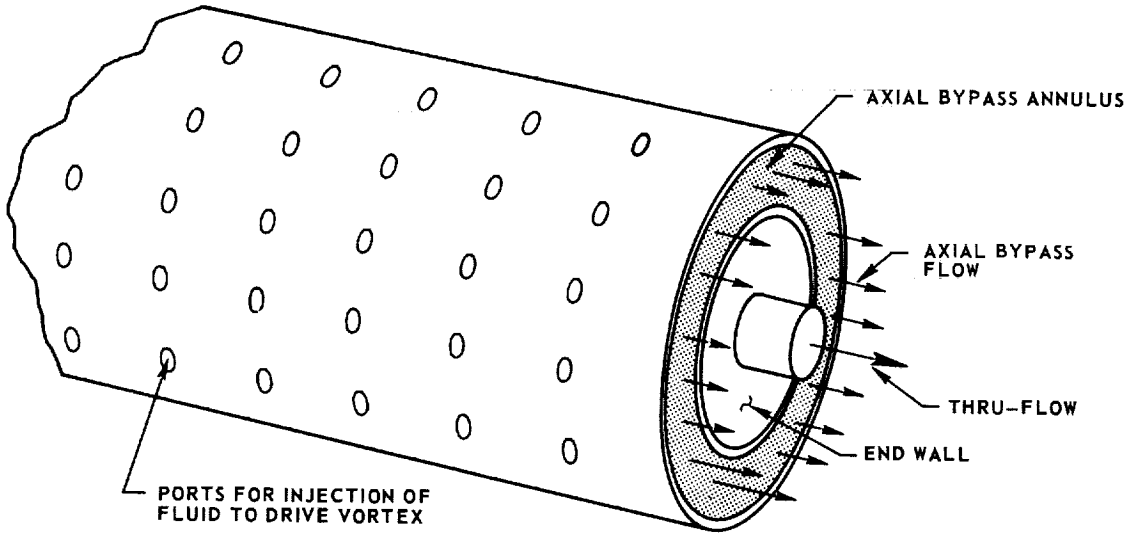

JET–INJECTION VORTEX TEST APPARATUS

TESTED WITH BOTH PERIPHERAL BYPASS (REF. 10) AND AXIAL BYPASS

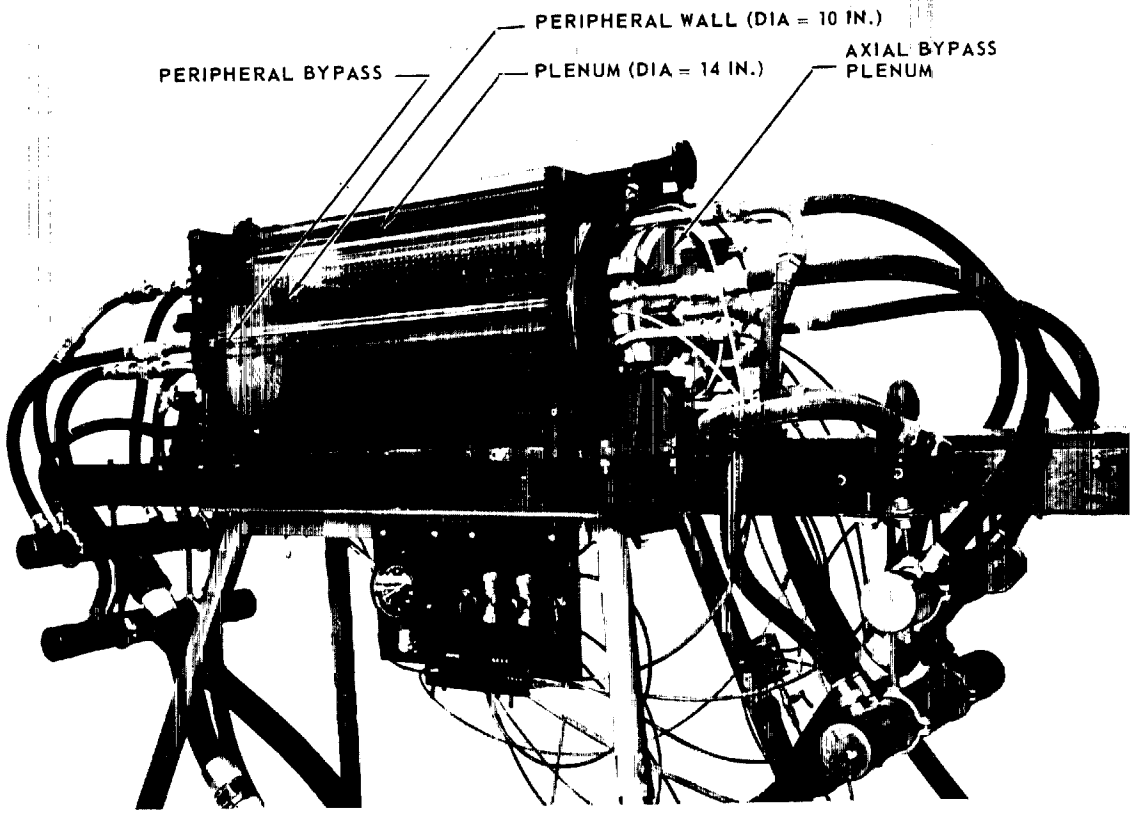

FIG. 4

FIG. 5

ROTATING-PERIPHERAL-WALL VORTEX TEST APPARATUS

TESTED WITHOUT BYPASS ONLY

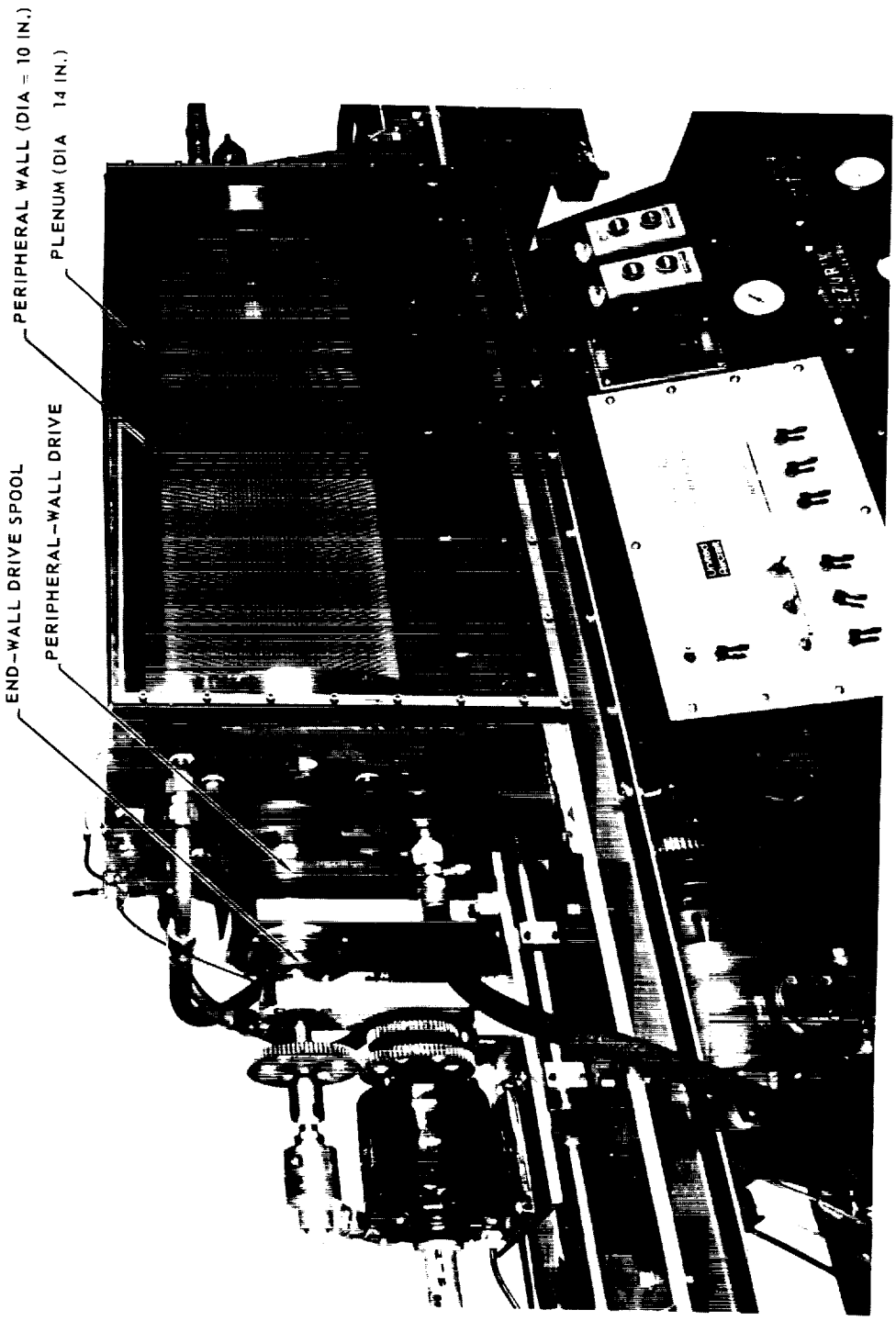

DETAILS OF VORTEX TUBES AND INJECTION CONFIGURATIONS

a) JET-INJECTION VORTEX TUBE

PERIPHERAL-WALL INJECTION AREA, A_j-IN.^{2}	NUMBER OF PORTS	DISTRIBUTION OF PORTS
6.0	2144	36 ROWS DISTRIBUTED AROUND PERIPHERY
0.679	240	4 ROWS OF 60 PORTS 90 DEG APART
0.236	80	4 ROWS OF 20 PORTS 90 DEG APART
0.118	40	40 ROWS OF 10 PORTS 90 DEG APART

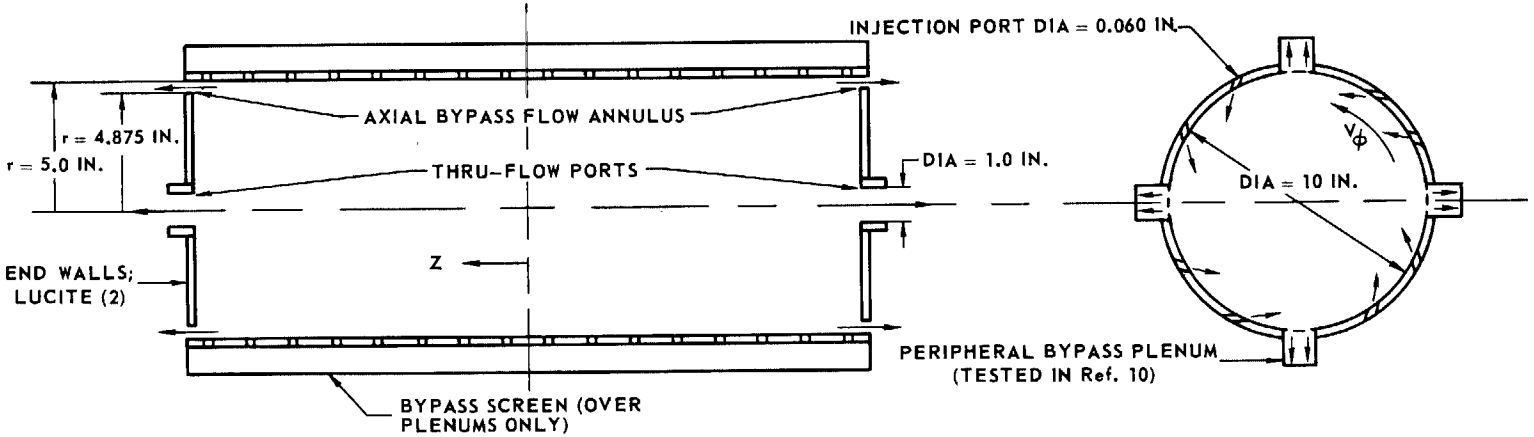

b) ROTATING-PERIPHERAL-WALL VORTEX TUBE

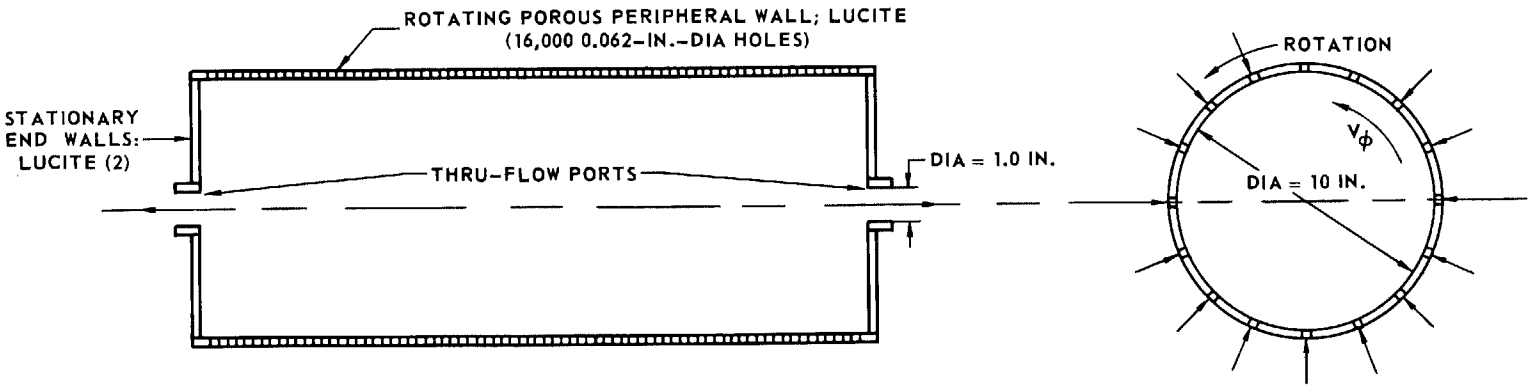

FIG. 6

OPTICAL SYSTEM USED TO OBTAIN DYE AND PARTICLE-TRACE PHOTOGRAPHS

NOTE: (1) FOR PHOTOGRAPHS TAKEN THROUGH END WALL (SEE SKETCH), ILLUMINATION OF DYE AND NEUTRALLY BUOYANT PARTICLES WAS BY LIGHT PASSING THROUGH AXIAL MID-PLANE

(2) FOR DYE PHOTOGRAPHS THROUGH SIDE OF VORTEX TUBE, LOCATIONS OF CAMERA AND LIGHT SOURCE WERE INTERCHANGED

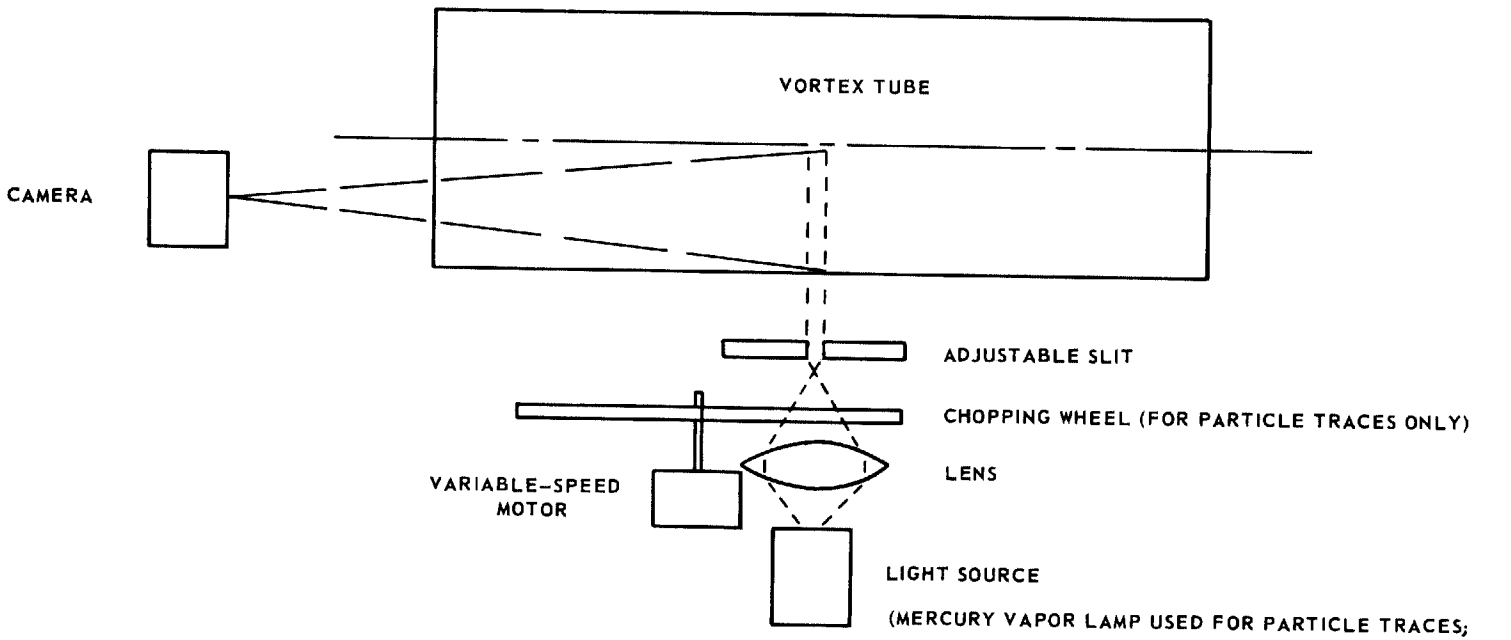

FIG. 7

FIG. 8

TYPICAL PARTICLE-TRACE PHOTOGRAPH

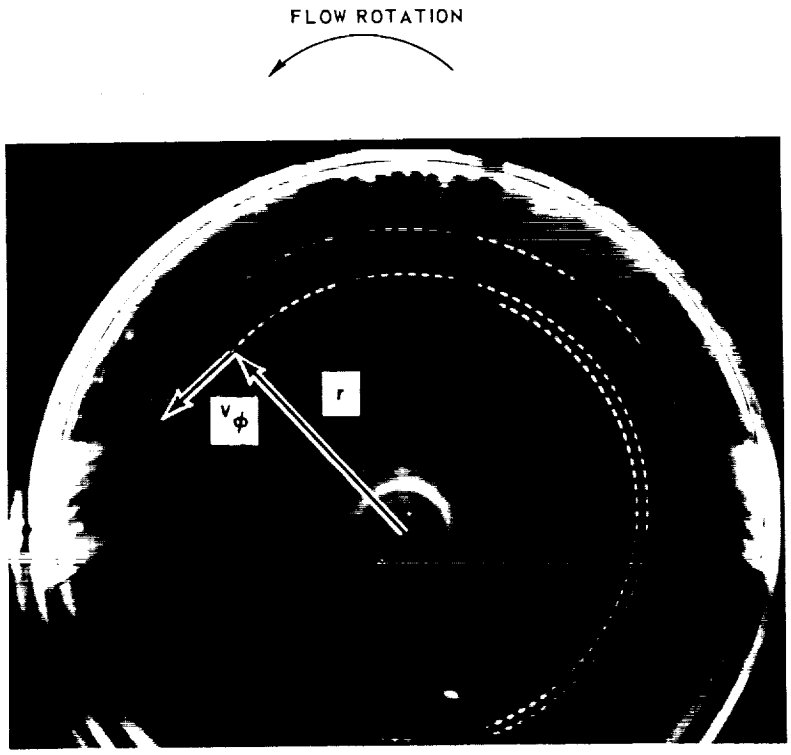

FIG. 9

APPROXIMATE VARIATION OF TANGENTIAL VELOCITY AT PERIPHERAL WALL WITH PERIPHERAL-WALL INJECTION AREA

JET-INJECTION VORTEX TUBE

DATA FROM EXTRAPOLATION OF VELOCITY PROFILES OBTAINED BY PARTICLE-TRACE METHOD

EACH DATA POINT IS AVERAGE FOR TESTS AT TWO VALUES OF $Re_{t,j}$

SYMBOL	PERIPHERAL-WALL INJECTION AREA, A_j, IN.^{2}	TANGENTIAL INJECTION REYNOLDS NUMBERS, $Re_{t,j}$	VOLUME FLOW RATE THROUGH INJECTION JETS, Q_j, gpm
○	6.0	80,000	60
		270,000	180
□	0.679	144,000	8
		620,000	34.5
△	0.236	415,000	8
		1,246,000	24
◇	0.118	714,840	7
		1,244,000	12

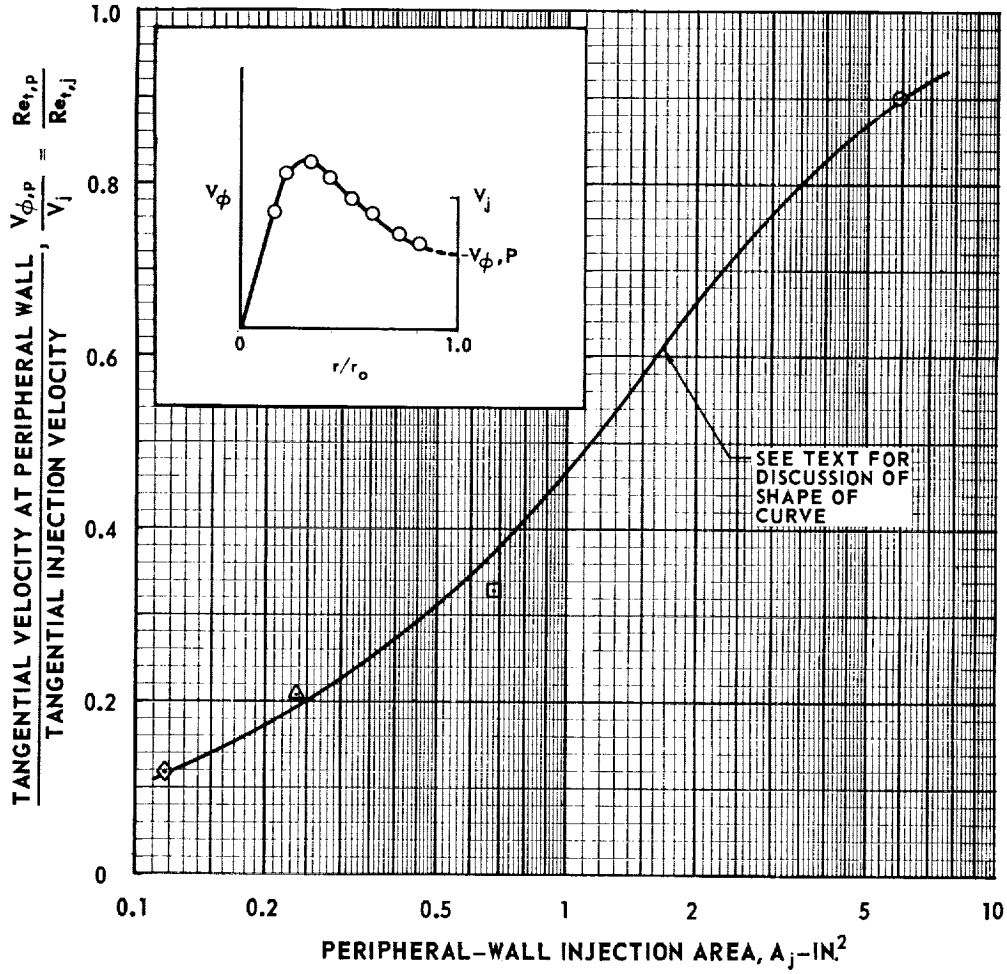

FIG. 10

TYPICAL DYE PATTERNS ILLUSTRATING EFFECT OF AXIAL BYPASS ON RADIUS OF RADIAL STAGNATION SURFACE

JET-INJECTION VORTEX TUBE

SEE FIG. 6a FOR DETAILS OF INJECTION CONFIGURATION

PERIPHERAL-WALL INJECTION AREA, $A_j = 0.679$ IN.^{2}

$Re_{t,j} = 144{,}000$; $Re_{t,p} = 47{,}500$

FLOW ROTATION

a) NO BYPASS

$Re_r = 102.5$; $\beta_t = 18.00$; $r_s/r_o = 0.30$

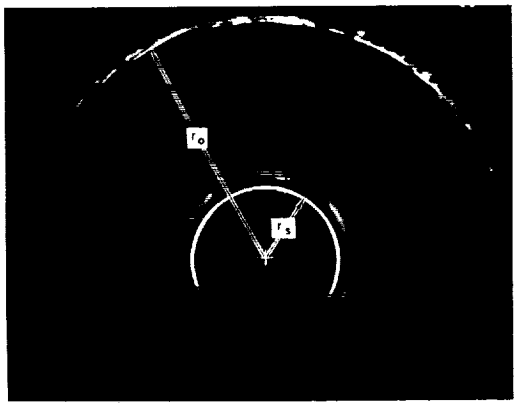

b) PERCENT BYPASS, $(Q_{BP}/Q_j) \times 100 = 15\%$

$Re_r = 87.2$; $\beta_t = 21.10$; $r_s/r_o = 0.44$

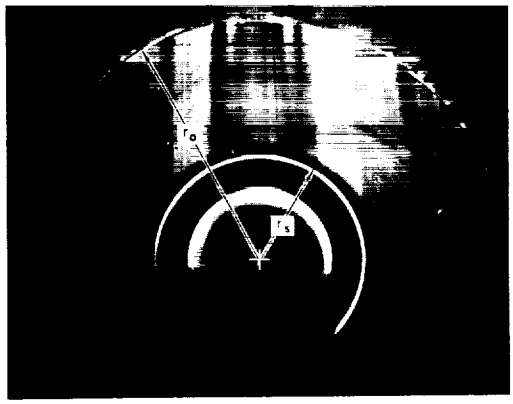

c) PERCENT BYPASS, $(Q_{BP}/Q_j) \times 100 = 40\%$

$Re_r = 61.5$; $\beta_t = 30.00$; $r_s/r_o = 0.68$

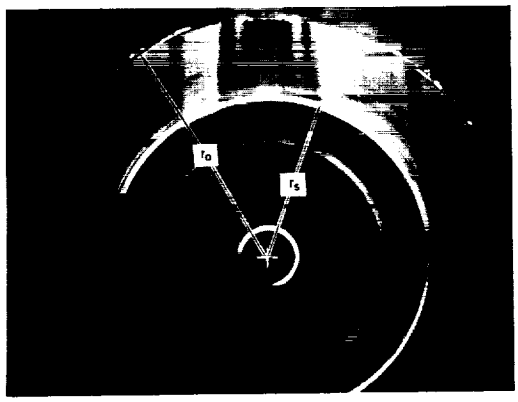

d) PERCENT BYPASS, $(Q_{BP}/Q_j) \times 100 = 65\%$

$Re_r = 35.9$; $\beta_t = 51.30$; $r_s/r_o = 0.70$

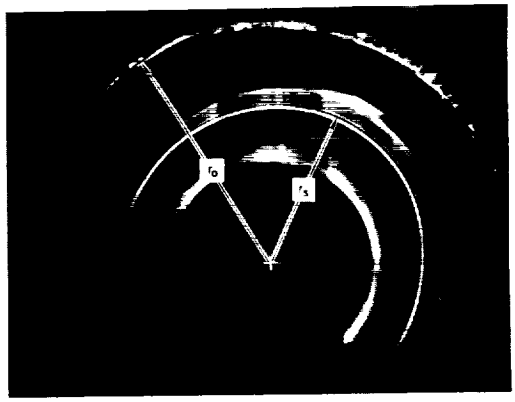

EFFECT OF PERIPHERAL-WALL INJECTION AREA AND PERCENT BYPASS FLOW ON RADIUS OF RADIAL STAGNATION SURFACE

JET-INJECTION VORTEX TUBE

RANGES OF FLOW CONDITIONS: $8\times10^4 < Re_{t,j} < 1.8\times10^6$, $4.7\times10^4 < Re_{t,p} < 2.6\times10^5$
$20 < Re_r < 442$, $18 < \beta_t < 128$

SYMBOL	PERIPHERAL-WALL INJECTION AREA A_j, IN.^{2}	NUMBER OF PORTS	DISTRIBUTION OF PORTS
□	0.118	40	4 ROWS OF 10 PORTS, 90 DEG APART
△	0.236	80	4 ROWS OF 20 PORTS, 90 DEG APART
○	0.679	240	4 ROWS OF 60 PORTS, 90 DEG APART AND 12 ROWS OF 20 PORTS, 30 DEG APART
◇,▽	6.00	2144	36 ROWS DISTRIBUTED AROUND PERIPHERY

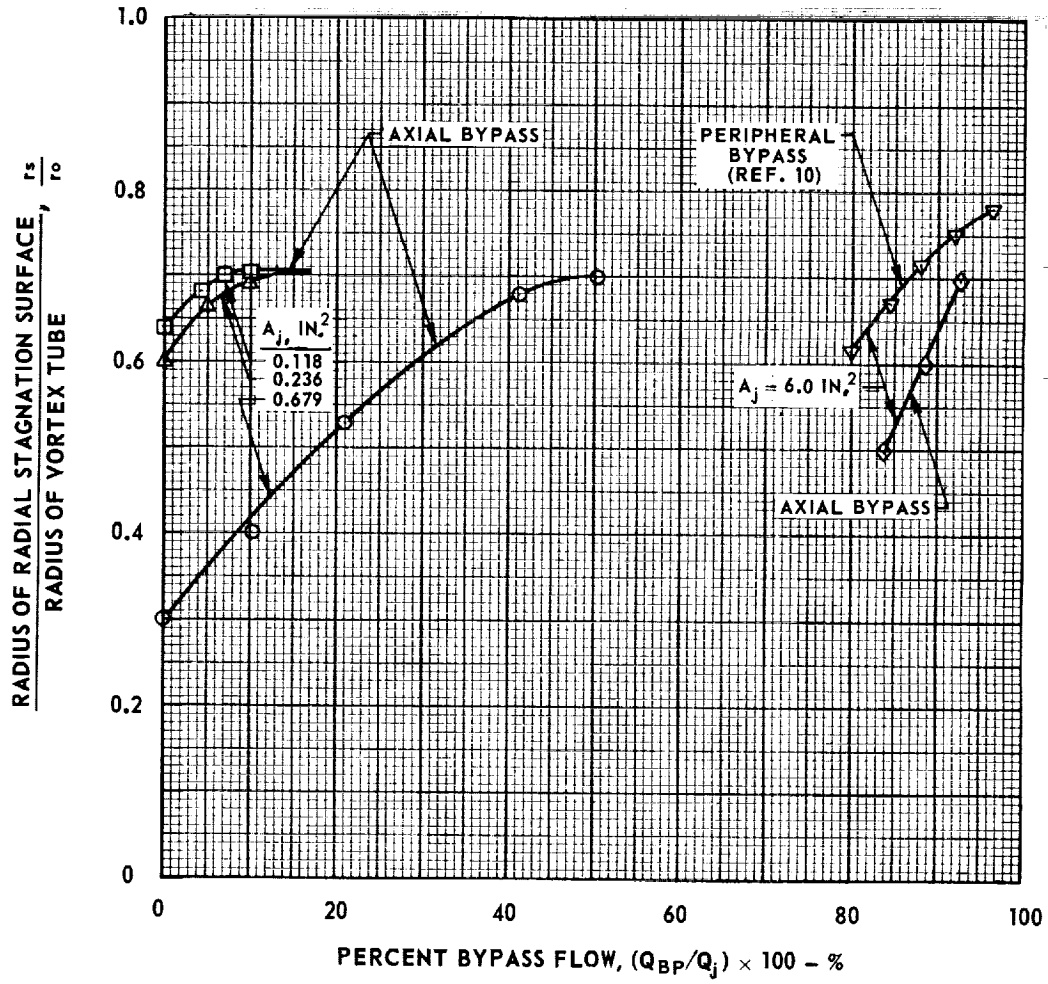

FIG. 12

TYPICAL DYE PATTERNS ILLUSTRATING WAVES IN RADIAL STAGNATION SURFACE

JET-INJECTION VORTEX TUBE

PERIPHERAL-WALL INJECTION AREA, A_j = 6.0 IN.^{2}

SEE FIG. 6a FOR DETAILS OF INJECTION CONFIGURATION

Re_r = 100 ; $Re_{t,j}$ = 120,000 ; $Re_{t,p}$ = 108,000 ; β_1 = 42

PERCENT BYPASS = 88% ; $\bar{V}_Z / V_{\phi,P}$ = 0.0676

PHOTOGRAPHS TAKEN THROUGH FRONT OF VORTEX TUBE AT DIFFERENT TIMES, t, AFTER CESSATION OF DYE INJECTION

DIRECTION OF AXIAL FLOW OUTSIDE OF RADIAL STAGNATION SURFACE

a) $t \approx 20$ SEC

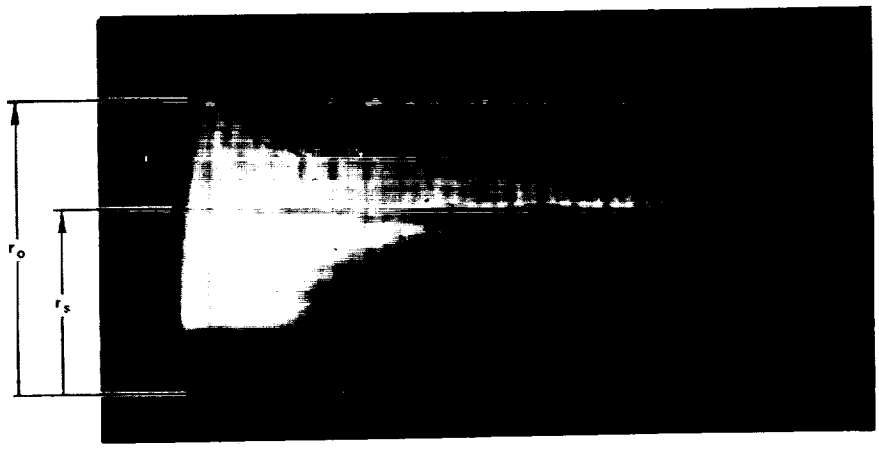

b) $t \approx 40$ SEC

FIG. 13

SUMMARY OF FLOW CONDITIONS FOR WHICH WAVES IN RADIAL STAGNATION SURFACE WERE OBSERVED

SEE FIG. 6 FOR DETAILS OF INJECTION CONFIGURATIONS

FLAGGED SYMBOLS DENOTE FLOW CONDITIONS FOR WHICH WAVES WERE OBSERVED

$$\bar{v}_z = \frac{Q_z}{\pi (r_o^2 - r_s^2)}$$

SYMBOL	A_j–IN.^{2}	BYPASS CONFIGURATION	VORTEX TUBE	$Re_{t,p}$
●	6.0	PERIPHERAL BYPASS (REF. 10)	JET–INJECTION	72,000
○	6.0	AXIAL BYPASS		108,000
△	0.679			47,500
×	0.236			131,000
□	0.118			85,780
◇	——	NO BYPASS	ROTATING–PERIPHERAL–WALL	118,000*

* VALUE LISTED IS $Re_{t,o}$

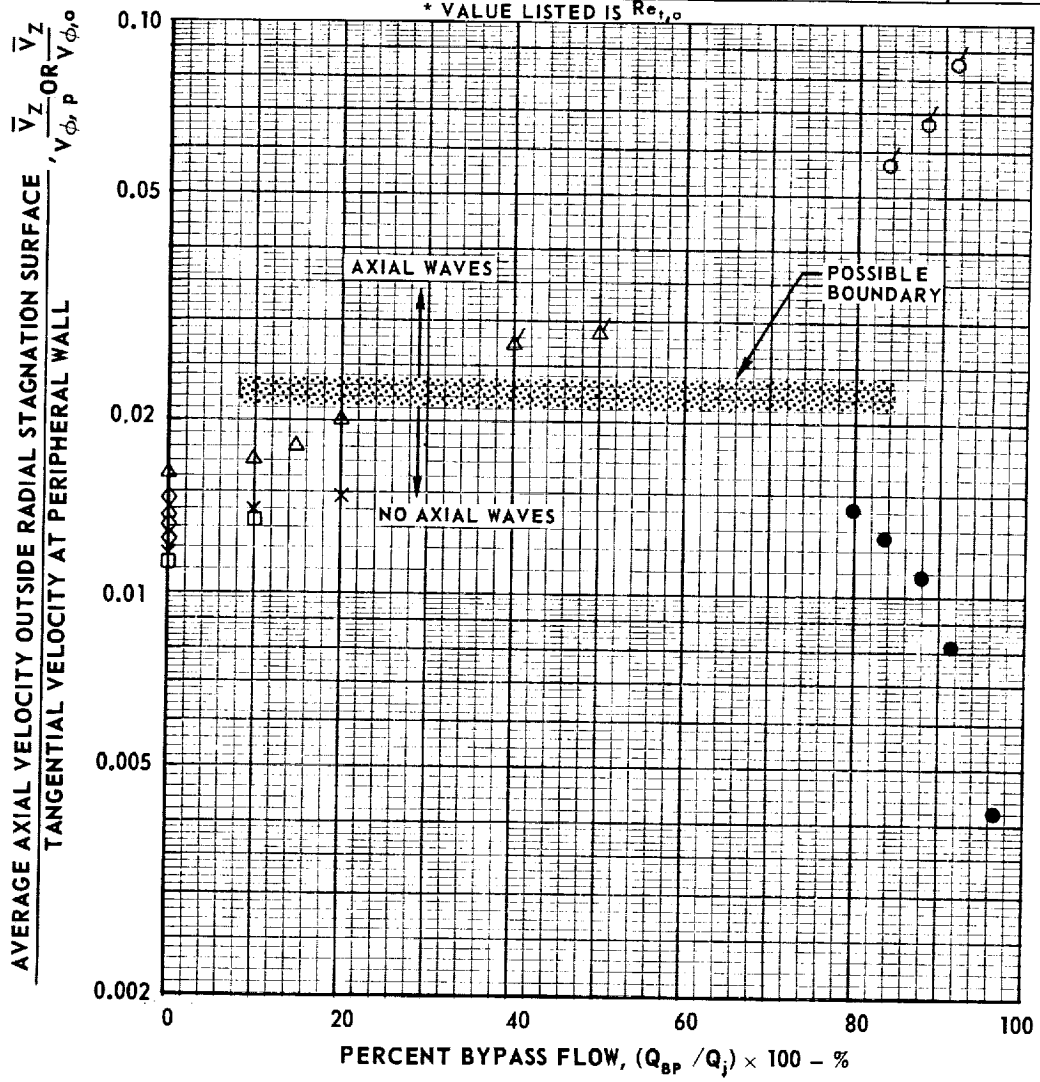

FIG. 14

TYPICAL DYE PATTERNS ILLUSTRATING EFFECT OF PERIPHERAL-WALL INJECTION AREA ON RADIUS OF RADIAL STAGNATION SURFACE IN FLOWS WITHOUT BYPASS

JET-INJECTION VORTEX TUBE

SEE FIG. 6a FOR DETAILS OF INJECTION CONFIGURATIONS

Re_r 102.5

FLOW ROTATION

a) PERIPHERAL-WALL INJECTION AREA, A_j 0.679 IN.^{2}

$Re_{t,j}$ 144,000 ; $Re_{t,p}$ 47,500;

r_s/r_o 0.3 ; β_t 18.00

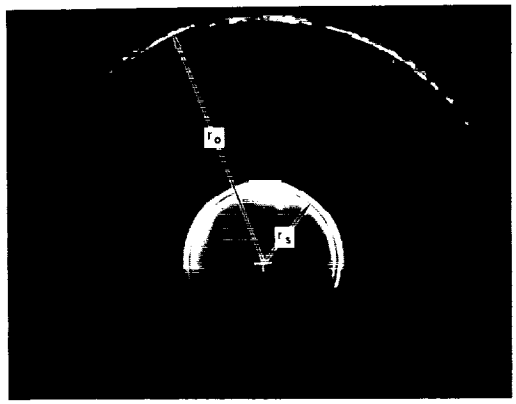

b) PERIPHERAL-WALL INJECTION AREA, A_j 0.236 IN.^{2}

$Re_{t,j}$ 415,000 ; $Re_{t,p}$ 87,200;

r_s/r_o 0.6 ; β_t 29.15

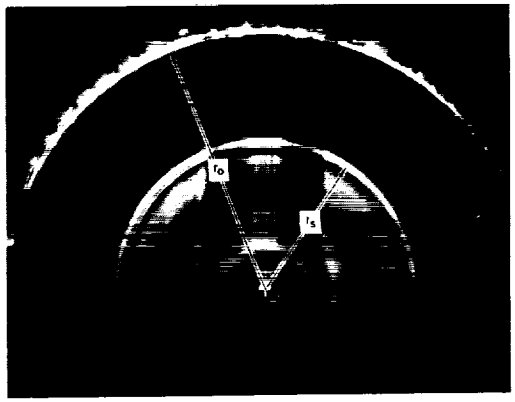

c) PERIPHERAL-WALL INJECTION AREA, A_j 0.118 IN.^{2}

$Re_{t,j}$ 1,244,000 ; $Re_{t,p}$ 149,400

r_s/r_o 0.64 ; β_t 29.65

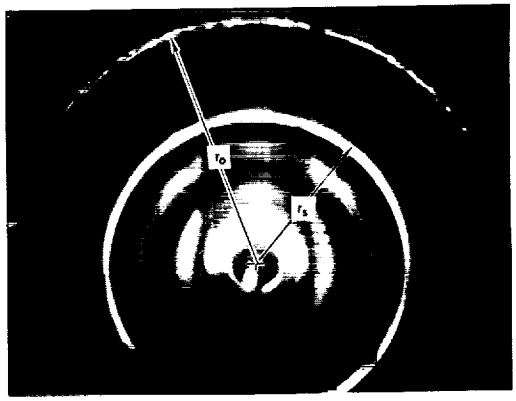

FIG. 15

TYPICAL DYE PATTERNS ILLUSTRATING EFFECT OF PERIPHERAL-WALL ROTATION RATE ON RADIUS OF RADIAL STAGNATION SURFACE IN FLOWS WITHOUT BYPASS

ROTATING-PERIPHERAL-WALL VORTEX TUBE

SEE FIG. 6b FOR DETAILS OF INJECTION CONFIGURATION

Re_r 131

FLOW ROTATION

a) ROTATION RATE, N_O 50 RPM

$Re_{t,o}$ = 82,000; β_t = 21.9;

r_s/r_o 0.62

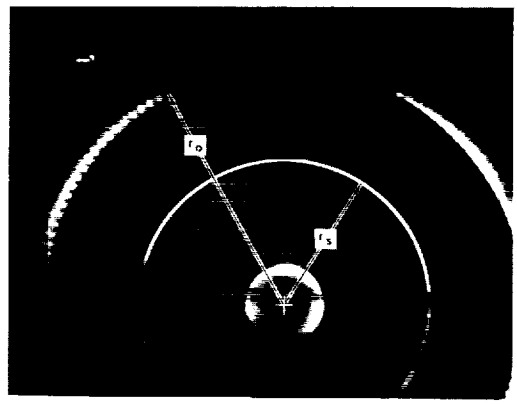

b) ROTATION RATE, N_O 90 RPM

$Re_{t,o}$ 150,000; β_t 35.2;

r_s/r_o 0.76

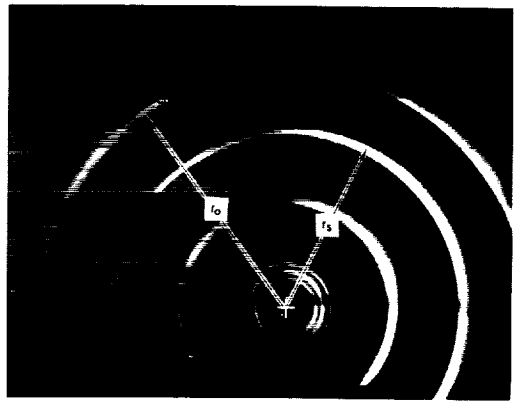

c) ROTATION RATE, N_O 130 RPM

$Re_{t,o}$ 214,000 ; β_t 46.7 ;

r_s/r_o 0.85

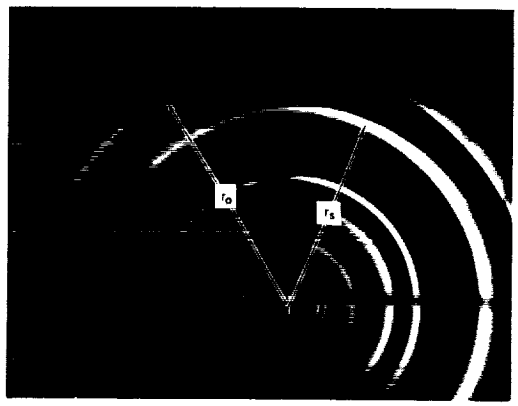

FIG. 16

EFFECT OF SECONDARY FLOW PARAMETER ON RADIUS OF RADIAL STAGNATION SURFACE IN ROTATING-PERIPHERAL-WALL VORTEX TUBE

NO BYPASS FLOW

N_0 = 40–145 RPM

$Re_{t,o}$ = 67,000–244,000

SYMBOL	Re_r
×	97
△	112
○	131
▽	154

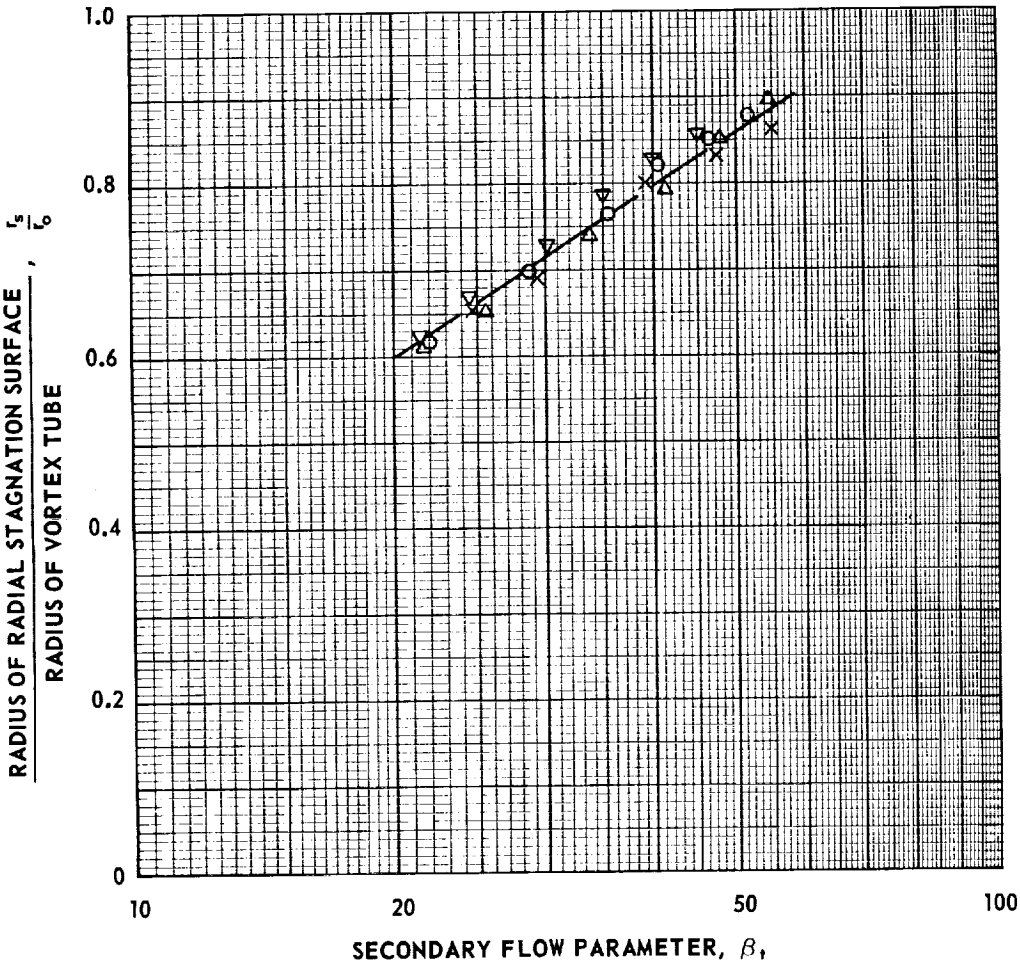

FIG. 17

COMPARISON OF MEASURED AND THEORETICAL RADII OF RADIAL STAGNATION SURFACES

SEE FIG. 6 FOR DETAILS OF INJECTION CONFIGURATIONS

SYMBOL	A_j – IN.^{2}	BYPASS CONFIGURATION	VORTEX TUBE
◇	—	NO BYPASS	ROTATING–PERIPHERAL–WALL
○	6.0	PERIPHERAL BYPASS (REF. 10)	JET–INJECTION
×	6.0	AXIAL BYPASS	
△	0.679		
□	0.236		
●	0.118		

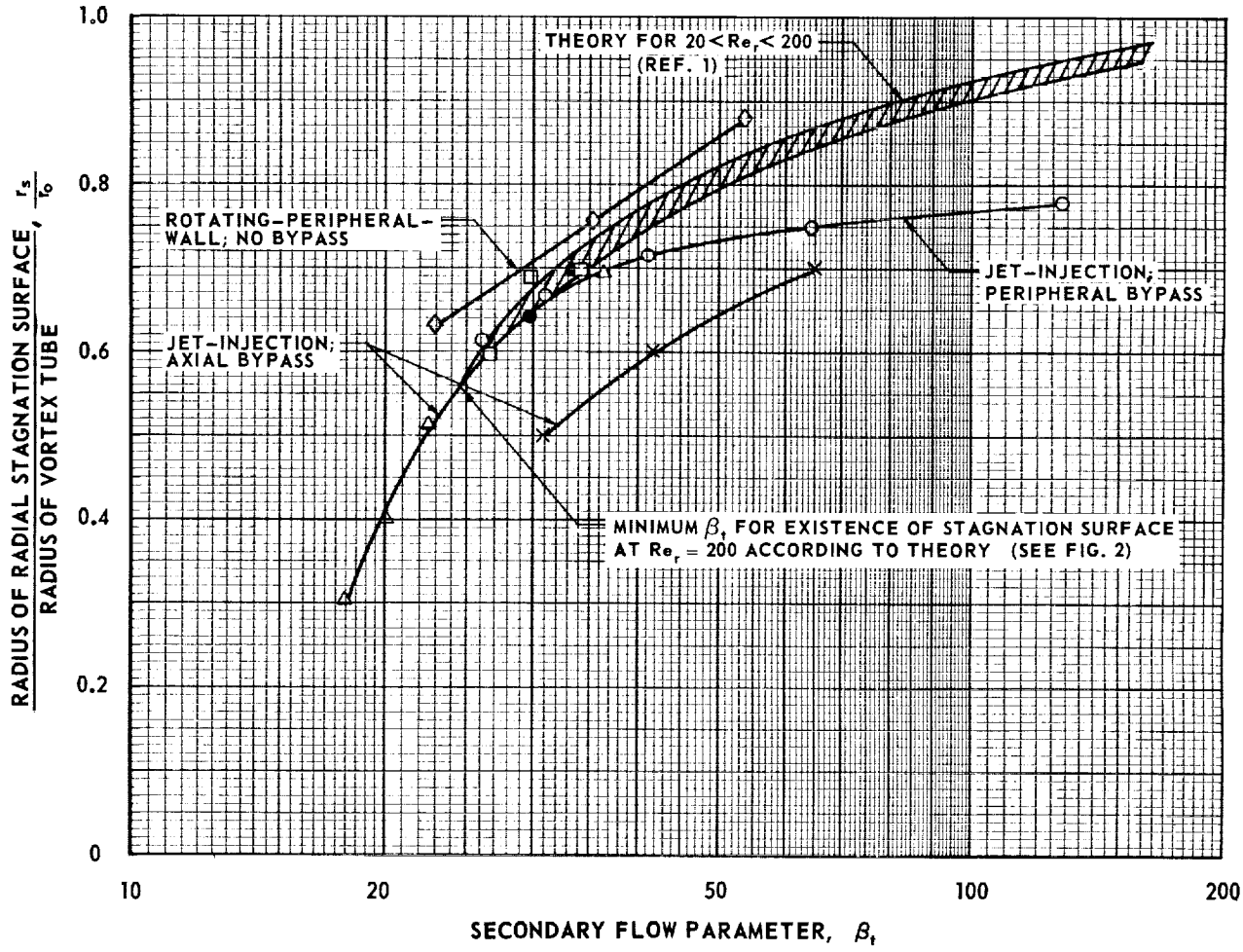

NASA-Langley, 1968 — 22 CR-1028